ADVANCED MATERIALS TECHNOLOGIES
www.advmattechnol.de

Combining Hydrophilic and Hydrophobic Materials in 3D Printing for Fabricating Microfluidic Devices with Spatial Wettability

*Max J. Männel, Niclas Weigel, Nicolas Hauck, Thomas Heida, and Julian Thiele**

The fabrication of microfluidic flow cells via projection micro-stereolithography (PμSL) has excited researchers in recent years. However, due to the inherent process properties of most commercial PμSL, microfluidic devices are fabricated in a monolithic fashion with uniform material properties across a flow cell. Yet, the large surface-to-volume ratio in microfluidics demands to tailor microchannel surface properties—particularly in planar microchannel arrangements—with spatial control and micron-scale resolution to form a desired flow profile, e.g., emulsion droplets. Here, the fabrication of planar microfluidic devices by PμSLbased 3D printing with spatial control over surface properties is presented. For that, homemade photopolymer formulations being either hydrophilic or hydrophobic are designed. Adding acrylic acid to a resin containing poly(ethylene glycol) diacrylate lowers the contact angle down to 0° against water creating a superhydrophilic surface. By utilizing 1*H*,1*H*,2*H*,2*H*-perfluorodecyl acrylate, a photopolymer formulation allowing for 3D-printing a hydrophobic microchannel surface with a contact angle >120° against water is obtained. Combining these two materials, microfluidic flow cells with spatially defined wettability are 3D-printed for emulsion formation. Finally, the resin vat of the commercial PμSL printer is switched during the printing process for fabricating multimaterial geometries, as exemplarily applied for realizing a hydrophobic-hydrophilic-hydrophobic device for forming O/W/O double emulsions.

1. Introduction

Over the last two decades, the common method for microfluidic device fabrication has been a combination of soft and photolithography based on poly(dimethylsiloxane) (PDMS).[1–3] PDMS is an ideal base material for microflow cell fabrication providing biocompatibility, optical transparency, and permeability to gases.[4] For example, transparency is a crucial requirement to follow the process of co-flow or microdroplet generation within a microfluidic flow cell with an optical setup. Yet, flow cell fabrication with PDMS involves several process steps that are prone to errors, especially by the user, and complex 3D-structures are difficult to produce, requiring multiple-layer fabrication that presupposes in-depth manufacturing experience. Therefore, researchers have started focusing on fabricating microfluidic flow cells via 3D printing due to its single-process character, short process time, and easy-to-distribute digital designs.[5–7] The interest in 3D printing of microfluidic flow cells has grown quickly indicated by a rapid increase in publications in this field.[8–12] In recent years, much effort has been put into investigating high-resolution 3D printing techniques to narrow the gap of achievable minimal feature sizes and functionality between PDMS-based and 3D-printed microfluidic devices. As one promising 3D printing technology, projection microstereolithography (PμSL) has gained great interest. Established microfluidic modules such as droplet generators,[13] valves,[14] and pumps[6] manufactured via PμSL have been reported. To more precisely tailor the functionality of 3D-printed microfluidics, photopolymer formulations have been developed to improve the transparency[15] and long-term biocompatibility of PμSL-printed cell culturing environments or biosensors.[16]

Another key application of microfluidics is the formation of uniform, picoliter-sized water-in-oil (W/O) and oil-in-water (O/W) emulsion droplets, as well as emulsions with more complex architectures, for example, droplets containing multiple immiscible cores.[17,18] Microfluidically prepared emulsions have been frequently used as templates for material design,[19] high-throughput screening,[20] genotyping,[21] blood tests,[22] and cell-free protein synthesis.[23]

Conventionally, in planar microflow cells with uniform microchannel height, the surface of channels needs to be functionalized to form a specific wettability for generating a desired type of emulsion. Exemplarily, for producing W/O emulsions,

M. J. Männel, N. Weigel, N. Hauck, T. Heida, Dr. J. Thiele
Leibniz Institut für Polymerforschung Dresden e.V.
Hohe Str. 6, 01069 Dresden, Germany
E-mail: thiele@ipfdd.de
Dr. J. Thiele
Dresden Center for Intelligent Materials (DCIM)
Technische Universität Dresden
01069 Dresden, Germany

The ORCID identification number(s) for the author(s) of this article can be found under https://doi.org/10.1002/admt.202100094.

DOI: 10.1002/admt.202100094

channel walls have to be hydrophobic to minimize the contact between the microchannels and the dispersed, aqueous phase. Emulsion formation involving more than two phases, for example, double emulsions (water-in-oil-in-water, W/O/W, or oil-in-water-in-oil, O/W/O) require more complex, spatially defined control of wettability in different sections of the flow cell.[24]

In recent years, the general concept of emulsion formation has been successfully transferred from PDMS-based to 3D-printed microfluidics.[9,25,26] However, while the minimum droplet diameter commonly ranges from approx. 10 to 100 µm when employing conventional microfluidic devices for emulsion formation, the smallest droplet size of emulsions produced in 3D-printed drop makers has been limited to ≈80 µm due to the resolution of the 3D printing process and thus the corresponding channel cross-section.[9] Interestingly, ensuring optimal wettability between liquids and the surface of printed materials, as required for microemulsion formation, has largely not been considered in 3D-printing flow cells compared to PDMS-based microfluidics. Instead, due to the design flexibility of additive manufacturing, more complex, non-planar microchannel architecture has been implemented by PµSL.[27] In sharp contrast to a two-phase flow profile for droplet formation in simple planar microchannels, the flow profile in previously implemented non-planar microchannels consists of an inner-phase flow that is surrounded by the second, outer flow. The realization of this protective sheath flow in exemplary 3D-printed, non-planar microchannels allows for using one flow cell independent of the surface wettability of the microchannels or whether the inner, discontinuous phase for emulsion formation is oil-like or aqueous. Extending the concept of utilizing a non-planar microchannel junction for emulsion formation, double emulsions can be produced in the same fashion in 3D-printed flow cells by combining two non-planar droplet maker.[9] Yet, bypassing the need for spatially controlling surface wettability in a microfluidic device by utilizing non-planar microchannels comes at a cost. To accommodate a multi-phase sheath flow, the microchannel cross-section at the second junction is usually much larger and requires higher sets of flow rates for stable droplet formation compared to double-emulsion production in planar devices, which becomes an issue, if particularly rare or precious samples need to be processed via droplet microfluidics. Ideally, high-resolution 3D printing of easy-to-fabricate planar microchannels could be combined with spatial control over microchannel wettability.

A wide range of photopolymer formulations (resins) have been developed for microfluidic device fabrication via PµSL, being elastomeric, chemically resistant, transparent, and offering high resolution.[28,29] However, the surface wetting properties were previously largely not in the focus of research when attempting to combine 3D printing and droplet microfluidics.[30] Here, we introduce resins for PµSL, which allow for precisely tailoring the surface properties of 3D-printed polymer materials from hydrophilic to hydrophobic. As a hydrophilic resin, we utilize a formulation of poly(ethylene glycol) diacrylate (PEGDA) mixed with acrylic acid (AA) to adjust the contact angle against water. On the other hand, 1*H*,1*H*,2*H*,2*H*-perfluorodecyl acrylate (PPFDA) is mixed with 1*H*,1*H*,6*H*,6*H*-perfluoro-1,6-hexyl diacrylate (PFHDA) to serve as the base materials of the hydrophobic resin. We expect the concept of mixing small amounts of AA into a resin to render the surface wettability hydrophilic to be transferrable to other photopolymer formulations to adjust their contact angle without losing their inherent properties.[31]

Despite being dissimilar among each other concerning their wettability, we establish a step-by-step PµSL process routine in which the first hydrophilic material is 3D-printed onto another hydrophobic resin. To combine polymer materials with different wettability within the same 3D-printed layer, we change the photopolymer formulations while printing single layers. With that, we locally change the surface wettability in a 3D-printed polymer material with micrometer-precision, which provides the basis to not only fabricate microfluidic devices with planar microchannel cross-junctions for single-emulsion formation but to produce double emulsions. For that, we design a first drop maker to be hydrophilic and a second drop maker to be hydrophobic. This enables the first drop maker to produce oil droplets in water and at the second junction, the oil-in-water droplets are encapsulated in another phase of oil leading to the formation of O/W/O double emulsions.

2. Experimental Section

2.1. Materials and Methods

Diphenyl(2,4,6-trimethylbenzoyl)phosphine oxide (TPO), PEGDA ($\overline{M_w}$ = 250 g mol^{-1}), Sudan 1, AA (99%), Pluronic F-127, and Triton X-100 were purchased from Sigma-Aldrich (Germany). PFHDA (95%) and PPFDA (97%) were bought from abcr GmbH (Germany), hydrofluoroether (HFE) 7500 from IoLiTec (Germany), and Krytox FSH from Costenoble GmbH & Co. KG (Germany). Acetone, *n*-hexadecane (99%), ethanol (99.5%, EtOH), isopropyl alcohol (IPA), tetrahydrofuran (THF), dimethylformamide (DMF), chloroform, dichlormethane (DCM), and toluene were purchased from Acros Organics (United States). All chemicals were used without further purification unless otherwise stated. Deionized water (DI-water) was prepared in a Milli-Q-Direct 8 instrument with a resistivity of 18.2 MΩ cm^{-1}. Graphical data evaluation was performed using IGOR Pro (Version 6.3.7.2., Wave Metrics, Inc., Oregon, United States).

3D-printed samples made of resin formulation (RF) RF 2 and RF 3 with a thickness of 1 mm were placed into a 96-well plate (polystyrene) and inserted into a plate reader (Infinite 200 Pro, TECAN). Five samples of both resins were measured regarding their absorbance A at wavelengths from 300 to 900 nm with 3 nm steps at 15 flashes. Three spots were measured without the sample being the average blank measurement. To determine the transmittance of the 3D-printed object, the blank measurement was subtracted from the sample measurement. The transmittance was then calculated by $T = 10^{-(A)} \times 100$, and averages transmittances with their respective standard deviation are illustrated in the Supporting Information.

Scanning Electron Microscopy (SEM) images and energy-dispersive X-ray spectroscopy (EDX) maps were acquired with a Ultra Plus SEM (Carl Zeiss AG, Oberkochen, Germany) operated at acceleration voltage of 3 kV and equipped with a XFlash

Table 1. Resin formulations developed for the study at hand. Resin formulation (RF) 1 and 2 are based on PEGDA, Sudan 1, and TPO while RF 3 is based on PPFDA.

Resin formulation (RF)	PEGDA	PPFDA	PFHDA	Acrylic acid	Sudan 1	TPO
RF 1[a)]	98.6				0.4	1
RF 2	98.5			0.1	0.4	1
RF 3		94.425	5		0.075[b)]	0.5

All units are in % (w/w); [a)]Resin formulation is adapted from Gong et al.;[6] [b)]Beforehand, Sudan 1 is dissolved in acetone with a concentration of 50 mg mL^{-1} before addition to PPFDA.

5060 EDX detector (Bruker Nano GmbH, Berlin, Germany). The flat surface for SEM imaging was cut by a diamond knife using a UC6 ultramicrotome (Leica Microsystems GmbH, Wetzlar, Germany). Prior to SEM imaging, the specimen was coated by ≈20 nm carbon film (SCD500 coater, Leica Microsystems GmbH, Wetzlar, Germany) to prevent charging under the electron beam.

2.2. Photopolymer Formulations

Typically, photopolymer formulations consist of a monomer or macromer that can be polymerized by UV-induced radical polymerization, a UV-absorber, a photoinitiator, and a cross-linker, if the macromer cannot act as a cross-linker on its own. Traditionally, base materials are (multi-functionalized) low molecular-weight acrylates due to their liquid state at room temperature. By using di- or tri-functionalized instead of monofunctional acrylates, a cross-linker is not required as the monomer can serve as a cross-linker itself. Based on these considerations, photopolymer formulations based on different cross-linkable base materials (PEGDA, PPFDA, PFHDA), Sudan 1 as UV-absorber, TPO as photoinitiator (**Table 1**), and AA as an additive were designed.

To ensure sufficient mixing of all components, the as-prepared resin formulations were treated by low-power ultrasonication for 20 min. Due to poor solubility of Sudan 1 in PPFDA and PFHDA, it was dissolved in acetone at a concentration of 50 mg mL^{-1} before adding it to the resin formulation. The resins were stored in amber glass bottles to avoid undesired polymerization before usage.

2.3. 3D Printing

For fabricating 3D-printed parts, an Asiga Pico 2 (Asiga Germany, Erfurt, Germany) with a lateral resolution of 39 µm, a maximum building volume of 51.2 mm × 32 mm × 75 mm in X-, Y-, and Z-direction, respectively, and a 385 nm light source was used. While the resolution in Z-direction can be varied by 1 µm increments, Nordin et al. showed that the minimum achievable lateral resolution is approx. 4 times the pixel pitch, which is 156 µm in this case.[6] The 3D objects were designed using the software Autodesk Inventor Professional 2020 (Autodesk Inc., San Rafael, United States). The computer-aided designs were converted into standard tessellation language (stl) files by the software for further use in the 3D-printing process. The location and orientation of the digital objects stored in the stl-files were further modified in the Asiga composer software. Different printing parameters can be adjusted within the software including layer thickness, exposure time, exposure intensity (here, an intensity of 100% is equal to 16.67 mW cm^{-2}), and the separation distance between resin vat and 3D-printed object. The duration time of the printing process primarily depended on the length of the designed object in Z-direction since the printing process proceeds in a layer-by-layer fashion. Exemplarily, an object with a height of 5 mm was 3D-printed within ≈30 min with a set layer thickness of 50 µm, a separation distance of 3 mm, and an exposure time of 3 s.

A typical microfluidic flow cell for single-emulsion formation was designed with a microchannel cross-section of 200 µm at the droplet-forming junction and the outflow channel. A scheme of the design is shown in Section 3.4. To ensure sufficient connection of the printed part and tubing feeding fluids into the flow cell during microfluidic experiments, cylinders with a diameter of 1.05 mm were designed to serve as fluid inflow ports—as commonly applied in microfluidics—without the need for additional adhesives. The typical total size of the flow cells was 5.8 mm × 11.3 mm × 13.7 mm in X-, Y-, and Z-direction, respectively, with the microchannel cross-junction being located 8.7 mm inside the design from the top surface in Z-direction. Importantly, several flow cells can be printed at the same time to efficiently fill up unoccupied area at the building platform. The channel dimensions inside the 3D-printed flow cells were obtained by bright-field microscopy from an Axio Vert.A1 (Carl Zeiss AG, Oberkochen, Germany) equipped with a 5x objective and a Phantom Miro C110 high-speed digital camera (Vision Research Inc., Wayne, United States).

After the printing process, to ensure sufficient removal of uncured and potentially trapped resin, the inflow ports of the 3D-printed flow cells were manually connected with tubing, and the channels flushed with water before drying the devices at 50 °C. Finally, the microfluidic devices were post-cured for 300 s with 10 UV-light flashes per second in an Otoflash G171 chamber (NK-Optik GmbH, Baierbrunn, Germany). To improve the optical transparency and the contrast in microfluidic experiments, a droplet of Krytox was placed between the 3D-printed object and a glass slide to follow droplet formation in situ.[9]

2.4. Dose Calibration

The investigation of optimal printing parameters was based on dose calibration experiments. For this, a film of uncured

resin was applied onto a glass slide, and dots with a diameter of 1.4 mm were exposed to UV-light for different time steps ranging from 1 up to 15 s. Uncured resin was removed by flushing with an appropriate solvent, and the glass slides were dried. The thickness of each dot was measured by confocal microscopy (Nanofocus Expert and μsoft metrology software for analysis, Nanofocus AG, Oberhausen, Germany), and the corresponding exposure energy E_{ex} was calculated by the equation:

$$E_{ex} = I_{ex} \times t_{ex} \quad (1)$$

Here, I_{ex} is the exposure intensity (16.67 mW cm^{-2}), and t_{ex} is the exposure time. By plotting the layer thickness against the exposure energy, the energy can be calculated for achieving a defined layer thickness.

2.5. Contact Angle Measurement

The static contact angle of different solvents (Milli-Q-water, HFE 7500, and hexadecane) on the surface of 3D-printed test objects was measured using an OCA instrument (Dataphysics Instruments GmbH, Filderstadt, Germany). 3D-printed blocks were cleaned with dust-free tissues before drying them with pressurized nitrogen to ensure a dust-free and water-free surface before contact angle determination. Using the OCA Software SCA 20 (Version 2), droplets with a volume of 5 μL were placed on the surface with a volume dosing rate of 0.25 μL s^{-1} and analyzed with the software. Each sample was measured five times to provide a range of the contact angle.

2.6. Solvent Resistance

The stability of 3D-printed parts was investigated by immersion into nine different solvents, namely Milli-Q-water, acetone, IPA, EtOH, THF, DMF, DCM, chloroform, and toluene. 3D-printed discs serving as test objects had a diameter of 10 mm and a height of 3 mm, as measured by bright-field microcopy, before immersion. After 24 h, the discs were removed from the solvent and their diameter was measured again. Any change in diameter indicated the resistance against swelling in the respective solvent. Additionally, images of the immersion solutions were recorded to visualize the potential release of unbound compounds such as Sudan 1 from the 3D-printed disc into the respective solvent. Finally, images of the discs were recorded to detect any damages of the discs caused by the swelling process. Each sample was prepared and measured three times.

2.7. Formation of Single Emulsions in 3D-Printed Flow Cells with Spatial Wettability

3D-printed flow cells made from hydrophilic and hydrophobic materials were fabricated in a two-step printing process. For forming W/O emulsions, Milli-Q water was used as the inner (dispersed) phase and ammonium salt of Krytox dissolved in HFE 7500 (1.8% w/w) was used as the outer (continuous) phase. Microchannels guiding the inner and outer phases toward the microchannel junction were 130 μm in width and height, and the outflow microchannel was 110 μm in width and height. Both phases were pumped into the device via connected tubings by high-precision syringe pumps (Harvard Apparatus Pump 11 Pico Plus Elite, Holliston, United States). The flow rates were set to Q_d = 400 μL h^{-1} for the inner phase and Q_c = 2000 μL h^{-1} for the outer phase. The formation of droplets was followed via bright-field microscopy, and the emulsion was collected in an Eppendorf tube (Eppendorf, Hamburg, Germany).

The process of O/W emulsion formation in a planar microfluidic device requires the exact opposite wettability inside the microfluidic device. The surface of the microchannels was adjusted to be hydrophilic by using RF 2 for 3D printing. HFE 7500 was used as the inner phase, and as the outer phase, Milli-Q-water was used with Triton X-100 ($c > 2.5 \times 10^{-4}$ M) as the surfactant. The flow rates were set to Q_d = 2000 μL h^{-1} for the inner phase and Q_c = 6000 μL h^{-1} for the outer phase.

2.8. Formation of Oil-in-Water-in-Oil Double Emulsions in 3D-Printed Flow Cells with a Hydrophobic–Hydrophilic–Hydrophobic Wettability Pattern

For forming O/W/O double emulsions as an example for a higher-order emulsion,[18] a flow cell with two droplet-forming microchannel junctions with overall dimensions of 13 mm × 6 mm × 5 mm in X-, Y-, and Z-direction, respectively, was designed with a cross-section of 400 μm at both junctions. The flow cell was divided into three parts. The first part contained the inflow fluid ports of the inner and the middle phase with a size of 6 mm × 6 mm in X, Y-plane. The second part was 3 mm × 6 mm in X, Y-plane, and contained an inflow port for the most outer phase. The third part contained the outflow flow channel with a size of 4 mm × 6 mm. A scheme of the flow cell can be found in Section 3.6. The first and the third part of the flow cell were 3D-printed with the hydrophobic photopolymer formulation RF 3, and the second part was 3D-printed with the hydrophilic resin RF 2 yielding a 3D-printed flow cell with hydrophobic–hydrophilic–hydrophobic wettability pattern.

Double emulsions were formed with a fluid combination adapted from Abate et al.[24] The ammonium salt of Krytox FSH was dissolved in HFE 7500 (1.8% w/w), and the surfactant Pluronic F-127 (1%, w/w) was dissolved in Milli-Q-water. To form O/W/O double emulsions, the oil phase was injected at the inner and outer fluid inflow port, while the aqueous phase was injected into the middle port. The flow rates were set to Q_i = 4000 μL h^{-1}, Q_m = 6000 μL h^{-1}, and Q_o = 8000 μL h^{-1}, respectively. By precisely synchronizing droplet formation at each microchannel junction, oil was encapsulated into the water at the first flow-focusing junction, and then, the as-formed O/W droplets were encapsulated into larger droplets of oil at the second junction yielding the desired O/W/O emulsion droplets.

3. Results

Precise spatial control over wettability on the micro-scale is important for a variety of applications—particularly in the field of microfluidics, exemplarily, for the formation of emulsions.

To obtain microfluidic devices via 3D-printing, which bear flow cell sections with different microchannel wettability, we develop resins yielding polymer materials that are either hydrophilic or hydrophobic. While most 3D-printed polymers based on acrylates have static contact angles ranging from 70° to 90°,[32] we aim for 3D-printed hydrophilic materials with a contact angle below 70° and hydrophobic materials with a contact angle equal to or greater than 90°, ensuring different wetting behavior comparing the two materials. By optimizing printing parameters and resin properties, we aim for printing objects with spatially controlled surface properties on the smallest scale of the 3D-printed object—that is a single voxel. Recently, the group of Roppolo utilized AA to reduce the contact angle of an acrylate polydimethylsiloxane copolymer in a post-functionalization process down to around 50°.[33] In addition, Frascella et al. also utilized AA by adding it beforehand to the photopolymer formulation. This way, they reduced the contact angle also to approx. 50°.[34]

3.1. A Poly(ethylene glycol) Diacrylate-Based Hydrophilic Material for Projection Micro-Stereolithography-Based 3D-Printing

State-of-the-art homemade photopolymer formulations are mainly based on PEGDA-250.[15,35,36] Previously, several research groups characterized their resin formulations regarding polymerization depth, minimum feature size, the impact of UV-absorber, and biocompatibility.[37–39] However, the surface wettability was largely omitted. We expect resins based on PEGDA to yield hydrophilic 3D-printed objects on which aqueous solutions spread easily as known for 3D-printed parts coated with PEG solutions.[32] Also, Rogers et al. showed for a similar photopolymer formulation based on PEGDA-258 that the contact angle against water is 55°.[40] Therefore, we formulate a resin based on PEGDA-250 combined with 0.4% (w/w) Sudan 1 as the UV-absorber, and 1% (w/w) TPO as the photoinitiator. However, against our expectations, the contact angle measured was ≈71° and, thus, significantly higher than we aimed for. To improve surface hydrophilicity by adjusting the contact angle toward lower values, the resin formulation was mixed with various amounts of AA ranging from 0.1% (w/w) up to 50% (w/w) (**Figure 1**, Table S1, Supporting Information) corresponding to values obtained from the literature for the design of hydrophilic PDMS surface functionalization.[18,24]

First, we investigate the dose calibration of our resin with AA increasingly replacing the base material PEGDA. For that, a film of uncured resin is exposed for a set of time intervals with a fixed intensity of 16.67 mW cm^{-2} by the UV source of the 3D printer. For each time interval, a small circle with a diameter of ≈1.4 mm is printed, and the height is measured by confocal microscopy. By multiplying the intensity with the exposure time, the exposure energy is obtained and plotted against the object height (Figure 1A). While for an amount of 0.1% (w/w) AA the lowest energy to achieve a polymerized cylinder is 33 mJ cm^{-2}, a higher energy of 60 mJ cm^{-2} is required for all other samples. Further, a maximum height of 172 µm is achieved (0.1% AA, w/w), and the polymerization depth decreases step-by-step from 140 µm (10% AA, w/w) over 90 µm (25% AA, w/w), down

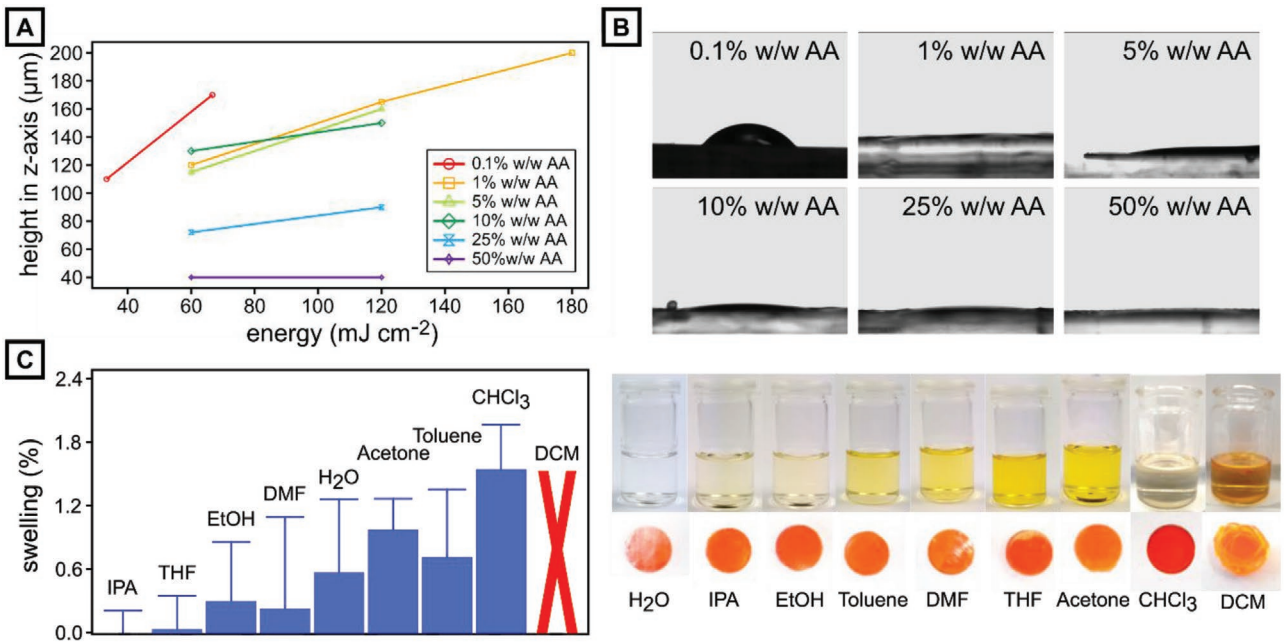

Figure 1. Characterization of photopolymer formulations for fabricating hydrophilic polymer objects via PµSL printing containing PEGDA-250, acrylic acid (AA), Sudan 1, and TPO. Characterization includes dose calibration, contact angle, and the swelling in organic solvents. A) The height of a 3D-printed layer is plotted against the respective UV-light energy. Lines between the data points are drawn as guide to the eye. B) The contact angle against Milli-Q-water on a 3D-printed surface drastically decreases from 0.1% (w/w) AA to 50% (w/w) AA, which serves as hydrophilic additive in the photopolymer formulation. C) Swelling of 3D-printed discs in nine different solvents after 24 h (H_2O, acetone, IPA, EtOH, THF, DMF, DCM, chloroform, toluene). Supernatants and 3D-printed discs after 24 h are shown in the right panel. Yellow color indicates the release of unbound Sudan 1 from the 3D-printed discs. The discs are destroyed in DCM and thus, no diameter could be measured.

to 42 μm (50% AA, w/w). More energy leads to over-curing of the circles and therefore, these points are not considered. One possible explanation for this trend is that by the substitution of PEGDA with AA, the di-functional PEGDA is replaced by mono-functional AA leading to faster polymerization due to the higher density of reactive groups. By the faster build-up of the polymer network, the mobility is lower and therefore, the propagating species is trapped in the network resulting in a smaller printed voxel. An additional test with pure acrylic acid mixed with Sudan 1 (0.25% w/w) and TPO (1% w/w) led to a spot with a discontinuous structure and uncontrolled height, confirming the necessity to include PEGDA in the photopolymer formulation for forming defined 3D-printed structures, such as flow cells, later on.

Second, we measure the contact angle for PEGDA-based resins containing different amounts of AA (Figure 1B). The lowest amount of 0.1% (w/w) already leads to a decrease in the contact angle from ≈71° for PEGDA-250 to ≈51°. Complete wetting with water (<5°) is achieved at 1% (w/w) AA, and no further change of the contact angle is observed in a range from 1% (w/w) to 50% (w/w) AA. However, we consider the addition of 0.1% (w/w) AA to be sufficient to change the surface property of a 3D-printed material from slightly hydrophilic (between 70° and 90°) to hydrophilic (≈51°), as higher amounts of AA lead to lower mechanical stability of the corresponding 3D-printed object as noticed in the printing process.[41] In addition, we also record an increase in object swelling in water. Moreover, the overall resin composition is hardly changed and thus expected to be comparable to well-studied PEGDA resins and their achievable polymerization depth and minimum feature size.

The solvent compatibility of 3D-printed polymer materials is crucial for many applications, for example, in (micro-) reactor and flow cell design for chemical synthesis or extraction and purification processes. Particularly, in the field of microfluidics, solvent compatibility is a major parameter in the design and application of microflow cells, as pioneered by Whitesides and coworkers in 2003.[42] To test the applicability of our resins for solvent-resistant flow cell fabrication, 3D-printed discs with a diameter of 10 mm and a height of 3 mm are prepared and stored in nine different solvents (Milli-Q-water, acetone, IPA, EtOH, THF, DMF, DCM, chloroform, and toluene) for 24 h. The increase in disc diameter is an indicator of the resistance of the 3D-printed material toward the specific solvent. Images of the discs and the solvents after 24 h of incubation time are shown in Figure 1C (right). We observe a change in solvent color from colorless to yellow for acetone, THF, DMF, chloroform, DCM, and toluene and light-yellowish for IPA and EtOH. Only water remains colorless. As we discussed in previous publications, the change in color originates from a release of Sudan 1 due to the swelling of these discs.[16,28] In the lower row of Figure 1C, the discs are shown after immersion. While the discs are mechanically stable for eight out of nine tested solvents, the disc immersed in DCM decomposes for each sample. Interestingly, the 3D-printed material based on PEGDA shows the highest swelling of ≈2% in chloroform. Finally, the transmittance of the resin after 3D-printing is approx. 70% (Figure S1, Supporting Information).

3.2. Design of a Fluorinated Resin for 3D-Printed Hydrophobic Surfaces

In previous work, we investigated a fluorinated photopolymer formulation with PFHDA, which yielded 3D-printed polymer materials with high resistance against common organic solvents.[28] However, the contact angle against water for this material is 84°, which is significantly lower than expected for a fluorinated surface. For instance, Tsibouklis and coworkers showed that a contact angle of water of 124° on a polymer film of poly(1*H*,1*H*,2*H*,2*H*-perfluorohexyl methacrylate) could be achieved.[43] Due to a similar chemical structure, we originally expected PFHDA to achieve a contact angle that is in the same range. We expect a higher amount of fluorine in a 3D-printed material should lead to improved hydrophobicity and thus contact angle values against water exceeding 84°. Therefore, in this study, PPFDA is introduced as a base material combined with a small amount of PFHDA as the cross-linker, Sudan 1 in acetone as the UV-absorber, and TPO as the photoinitiator. Similar to the investigation in Section 3.1, the dose calibration for different resin compositions and the evaluation of solvent resistance of 3D-printed test objects are performed (**Figure 2**).

The dose calibration is investigated for different mixtures of PPFDA and PFHDA either with UV-absorber (marked as diamond, hourglass, star, and pentagon) or without (circle, square, and triangle). First, mixtures of PPFDA and PFHDA (with PFHDA ranging from 10 to 99% w/w) without additional UV-absorber are tested to ensure the printability of the composition without demixing over time. All mixtures can be processed via PμSL (Figure 2A, circle, square, and triangle curve) with layer thicknesses ranging from ≈300 to 419 μm. As these values are too high to be considered as photopolymer formulations for 3D-printing with similar feature sizes as in conventional PDMS-based microfluidics—which we aim for—we add low amounts of Sudan 1, reducing the layer thickness significantly. While the addition of 0.025% (w/w) Sudan 1 leads to a layer thickness to 330 μm (diamond curve), a minimum layer thickness of 150 μm is obtained for a UV-absorber amount of 0.075% (w/w; star curve). On this account, the final photopolymer formulation contains 94.5% (w/w) PPFDA, 5% (w/w) PFHDA, 0.075% (w/w) Sudan 1, and 0.5% (w/w) TPO (pentagon curve). The film thickness increases linearly from 150 μm (E_{ex} = 94 mJ cm^{-2}) over 230 μm (E_{ex} = 141 mJ cm^{-2}) and 287 μm (E_{ex} = 188 mJ cm^{-2}) up to 361 μm (E_{ex} = 235 mJ cm^{-2}). The amount of PFHDA is decreased to 5% (w/w) compared to 10% (w/w) as before to ensure a high amount of fluorine provided by the backbone of PPFDA to further increase the contact angle against water.

In the next step, discs of 10 mm in diameter and 3 mm in height are 3D-printed with this resin composition and immersed in nine different solvents to test the solvent resistance (compare Section 3.1). We again measure the disc diameter before and after immersion for 24 h. Similar to the optimized hydrophilic resin (RF 2), the fluorinated resin shows no swelling in water and no leakage of photo-absorber into the supernatant. In IPA and EtOH, the material shows little swelling. The swelling in acetone, THF, and chloroform is most pronounced as previously observed for the hydrophilic RF 2, with an increase in disc diameter of 10.2% in THF. Compared

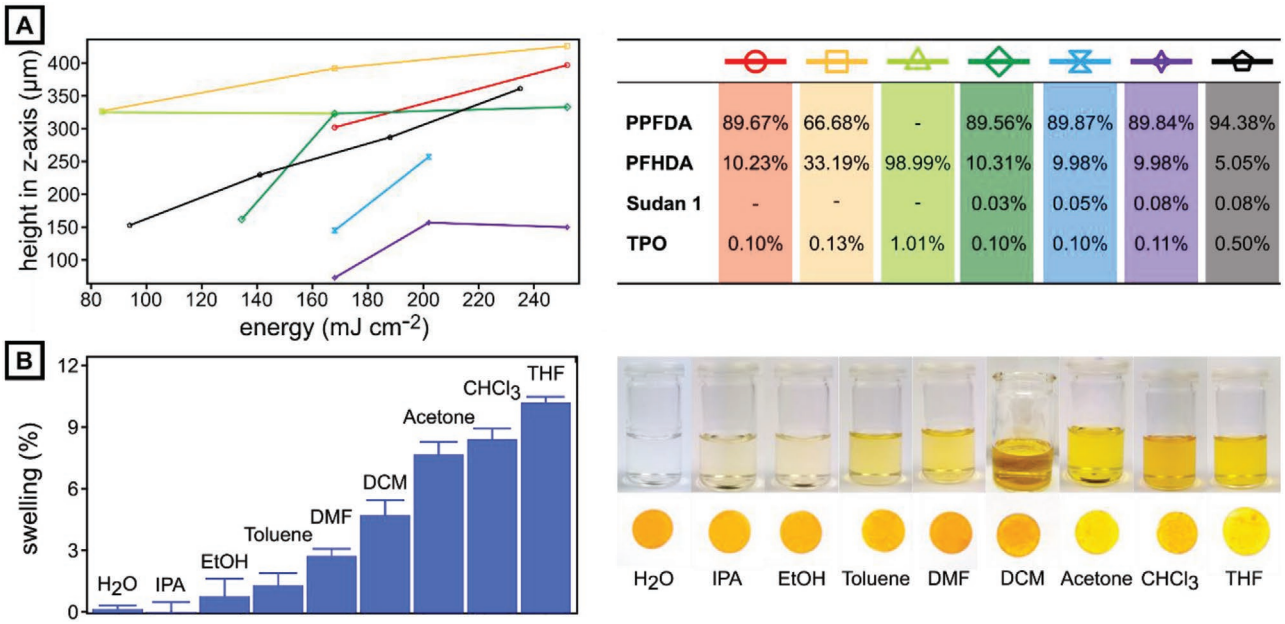

Figure 2. Photopolymer formulation for fabricating hydrophobic polymer objects via PµSL printing containing PPFDA, PFHDA, Sudan 1, and TPO, characterized regarding dose calibration and solvent resistance. A) The height of a 3D-printed polymer layer is plotted against the UV-light energy for different material compositions. B) Solvent resistance of 3D-printed discs made from a resin composed of 95% (w/w) PPFDA, 5% (w/w) PFHDA, 0.075% (w/w) Sudan 1, and 0.1% (w/w) TPO is tested for nine different solvents (Milli-Q-water, acetone, IPA, EtOH, THF, DMF, chloroform, toluene, and DCM). Left panel: Change in diameter of 3D-printed discs for each solvent. Right panel: Images of both, the discs after immersion and the supernatants.

to RF 2, no disc brakes during immersion, and all discs remain mechanically stable. For RF 3, we yield a sufficient solvent resistance toward Milli-Q-water, IPA, EtOH, DMF, DCM, and toluene, while the immersion in acetone, THF, and chloroform leads to significant swelling, yet no test prints break apart. The transmittance of 3D-printed objects made with this resin is approx. 80% (Figure S1, Supporting Information). Finally, we measure the distribution of the elements C, O, and F inside a printed cube via EDX. As shown in Figure S2, Supporting Information, the distribution is homogeneous for each element indicating no gradient formation of any element in the printing process.

3.3. Contact Angle Measurements

The contact angles of PµSL-printed polymer materials against Milli-Q-water, organic solvents, and fluorinated oils are of high interest since these liquids are commonly used for emulsion formation experiments in microfluidic devices to serve as the dispersed/inner phase or as the continuous/outer phase. On this account, we measure the contact angle of Milli-Q-water, hexadecane, and HFE 7500 on surfaces that are PµSL-printed from RF 1 (PEGDA, Sudan 1, and TPO), RF 2 (PEGDA, AA, Sudan 1, and TPO), and RF 3 (PPFDA, PFHDA, Sudan 1, and TPO) (**Figure 3**).

With an amount of 98.6% (w/w) PEGDA, the contact angle of RF 1 against water corresponds to a slightly hydrophilic surface with a contact angle of ≈71°, whereas we consider the change from hydrophilic to hydrophobic to be at ≈90°.[41] To reduce the contact angle, we add 0.1% (w/w) acrylic acid to RF 1 (named as RF 2). The addition of this small amount of acrylic acid leads to a decrease in the contact angle against water down to ≈51°. As we show in Section 3.1, a higher amount of acrylic acid will reduce the contact angle further causing perfect wetting of aqueous solutions and superhydrophilicity. Both photopolymer formulations show similar wettability against hexadecane as a reference for organic solutions with contact angles of ≈26° (RF 1) and ≈20° (RF 2), and they also exhibit a similar wetting toward fluorinated oils such as HFE 7500, where we achieve perfect wetting on 3D-printed surfaces made from RF 1 and RF 2.

In contrast, RF 3 is prepared to yield hydrophobic polymer objects via PµSL printing. By utilizing the fluorinated acrylate PPFDA at 94.5% (w/w), the contact angle against water increases to ≈127°. While the wetting of hexadecane is not very specific (≈67° against water), the fluorinated oil perfectly wets the surface made from RF 3. Interestingly, while we develop a set of resins that yield either hydrophilic or hydrophobic surfaces, HFE 7500 wets the surface of both resins perfectly. As discussed below, this very property is crucial for manufacturing 3D-printed parts from both resins joint together (Figure 3).

As this work aims for 3D-printing materials that are either hydrophilic or hydrophobic into a single object, we test the wetting of each uncured photopolymer formulation on already 3D-printed materials. Wetting is necessary to provide a sufficient contact area and thus binding between 3D-printed materials with different surface properties. For that, a block of RF 2 is printed and a droplet of both RF 2 and RF 3 is placed on the surface of the 3D-printed part (Figure 3, right upper corner). The contact angle of uncured RF 2 on the printed surface of RF 2 is ≈20°, and 13° for uncured RF 3. Both uncured photopolymer formulations thus wet well on the surface. Next,

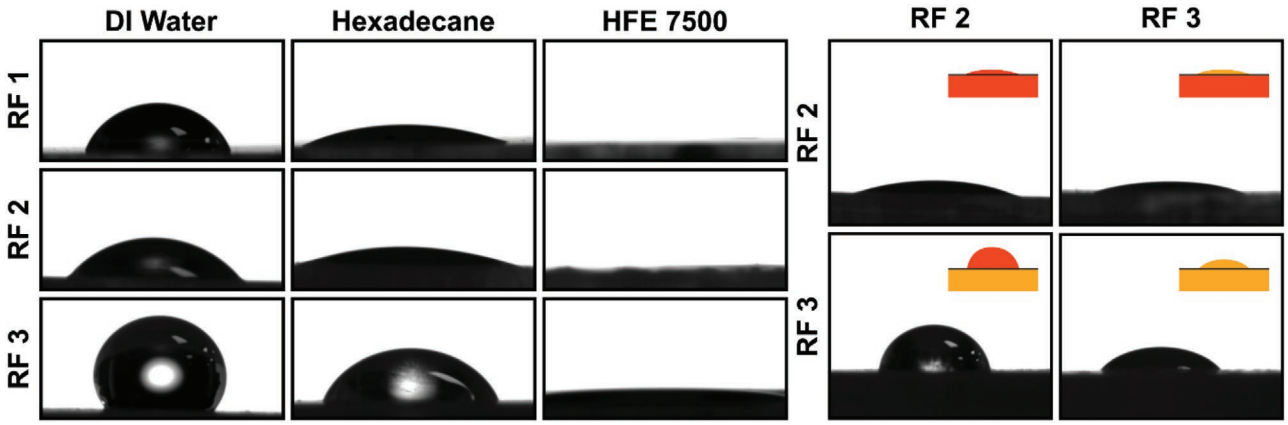

Figure 3. (Left) Three different resins for PμSL printing tested regarding their surface properties against the wetting of water, hexadecane, and HFE 7500. RF 1 exhibits a contact angle of ≈71° against water, ≈26° against hexadecane, and perfect wetting against HFE 7500 (top row). By changing the photopolymer formulation by the addition of 0.1% (w/w) acrylic acid, the contact angle decreases to ≈51° against water. The contact angle toward hexadecane and HFE 7500 does not change significantly (middle row). The fluorinated RF 3 shows excellent hydrophobic properties with a contact angle of ≈127° toward water (lower row). (Right) Wetting of RF 2 and RF 3 on the surface of each 3D-printed resin. In the upper row, a block made from RF 2 is 3D-printed, and the wetting of uncured RF 2 and RF 3 is shown. Both uncured resins wet the surface 3D-printed from RF 2 in a similar fashion with contact angles below ≈20°. For RF 3 (lower row), uncured RF 2 forms a contact angle of ≈83°, while uncured RF 3 naturally wets the surface of a 3D-printed block made from RF 3.

we investigate the wetting of uncured resins on a 3D-printed block of RF 3. Again, a droplet of either RF 2 or RF 3 is placed on the surface of the 3D-printed material made from RF 3. Here, a droplet of RF 2 forms a contact angle of ≈83°, thus the attachment of RF 2 on a 3D-printed surface made from RF 3 is not favored. In contrast, RF 3 attaches sufficiently to a surface made from the same material with a contact angle of ≈48°. Thus, while uncured RF 3 wets the surface of RF 2, it is not possible to process RF 2 and RF 3 in reverse order. Based on these findings, we consider both resins to be printable onto parts made from RF 2, while only RF 3 is processable on 3D-printed parts made from RF 3. These findings will be crucial for the later correct vat-switching during the 3D-printing process (compare Section 3.6). We have also considered to use a transitional resin (TR) that is miscible with both RF 2 and RF 3 to circumvent the wetting issue of RF 2 on RF 3. For that, we propose a mixture of PPFDA, PFHDA, and PEGDA (ratio 1:1:2 v/v, Figure S3, Supporting Information). Initially, a phase separation is directly visible that, however, disappears after vortexing the mixture. Thus, this resin mixture represents a potential TR. We assume that the miscibility can be adjusted by the amount of PFHDA in the mixture, since PFHDA is miscible with both, PEGDA and PPFDA. However, initial UV-curing tests with this very resin yield inhomogeneous, cloudy parts, indicating differently polymerized areas (Figure S3B, Supporting Information). Still, such a resin composition remains interesting for applications that do not require a sharp transition of wettability. However, in this manuscript, a sharp transition is mandatory to achieve reliable droplet formation.

3.4. Water-in-Oil Emulsion Formation in 3D-Printed Flow Cells with Hydrophilic–Hydrophobic Pattern

To prove that the afore-developed resin formulations can be printed together, we design a microfluidic flow cell for single-emulsion formation. For forming W/O emulsions in planar flow cells with uniform microchannel height, the surface of the microchannels should be hydrophobic from the droplet-forming junction onward. That way, wetting of the aqueous phase on the outflow channel's walls can be pushed back, particularly on the upper and lower wall, which may be insufficiently covered by the oil phase due to the squeezing of the aqueous phase from both sides at the droplet-forming microchannel cross.

In principle, single emulsions (W/O and O/W) can be fabricated inside microfluidic devices with uniform, spatially uncontrolled wettability. For instance, W/O emulsions form inside a hydrophobic flow cell such that the continuous oil phase wets the microchannel walls of the outflow channel and compartmentalizes the aqueous phase into droplets. In that case, the aqueous phase can be forced through the inflow channel toward the droplet-forming junction by a syringe pump or pressurized liquid reservoir independent of the microchannel surface properties in this part of the flow cell.

Yet, when utilizing simple flow cells with uniform microchannel height for forming multiple emulsions, which are smaller droplets resting inside larger droplets, e.g., W/O/W or O/W/O emulsions, spatially patterned microchannel wettability is vital; this allows inner drops to be formed in one part of the device and outer drops in another part. On this account, we first fabricate single-emulsion flow cells with spatially controlled wettability to investigate the principle of printing materials with different wettability together. For that, the first part of the flow cell is printed with the hydrophilic formulation RF 2 and the second part with the hydrophobic formulation RF 3. Following the findings from Section 3.3, we expect that RF 3 is printable on the surface of RF 2. The first part is printed with a layer thickness of 50 μm and an exposure time of $t_{ex} = 1.5$ s, which takes ≈30 min. Then, the second part is printed with the same layer thickness but an exposure time of $t_{ex} = 3$ s. The change of the resin is performed during the printing of

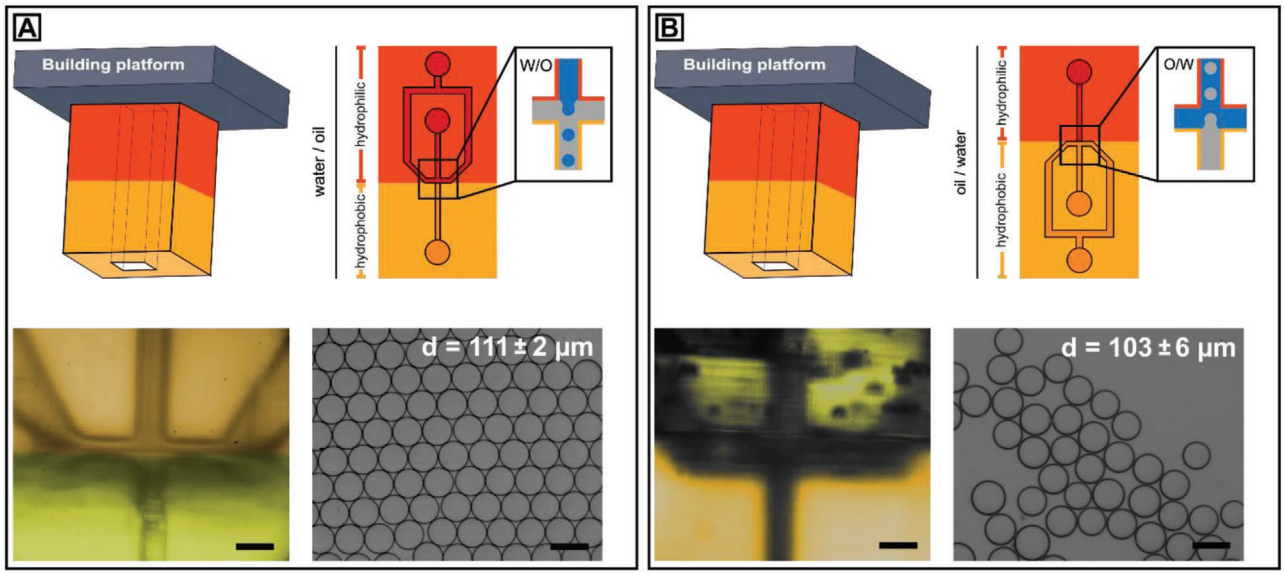

Figure 4. A) 3D-printed microfluidic flow cell consisting of a hydrophilic and a hydrophobic part. First, the hydrophilic part is printed at the building platform followed by printing the hydrophobic part onto the surface of the hydrophilic part. (Top right) Schematic of the microchannels residing inside the flow cell. To enable the formation of water-in-oil emulsions, surface wetting is adjusted to change from hydrophilic to hydrophobic properties at the junction (color-coded in the inset). (Bottom left) False-colored bright-field microscopy image highlighting the two material parts of the microfluidic device. (Bottom right) W/O emulsion generated with the flow cell with an average diameter of 111 ± 2 µm. B) O/W emulsion formation formed in a microfluidic flow cell with hydrophobic-hydrophilic surface patterning. The hydrophilic flow cell section containing the outflow channel is 3D-printed with RF 2 followed by 3D-printing the hydrophobic part including the inflow ports with RF 3. (Top right) Schematic of the different flow cell modules (hydrophopic section: light-yellow; hydrophilic section: orange). (Bottom left) Bright-field microscopy image of microfluidic junction artificially colored to highlight the different materials. (Bottom right) O/W emulsions with a diameter of 103 ± 6 µm produced in the flow cell. The scale bars denote 150 µm.

the microchannel cross-junction of the flow cell to ensure the presence of hydrophobic channel walls at the droplet-forming nozzle, thus avoiding any wetting of the aqueous dispersed phase on the walls and facilitating the generation of water-in-oil emulsions (**Figure 4**A).

In Figure 4, the scheme of the resulting flow cell is shown. The now upper part is hydrophilic and the lower part, where the outflow channel is located, is hydrophobic. A schematic of the surface pattern at the microchannel junction is shown in the inset of Figure 4A, where the aqueous phase is blue, and the organic phase is grey. A bright-field microscopy image focusing on the junction of the 3D-printed device is shown in Figure 4A (bottom left). The microchannel dimensions for the inner and outer phases leading toward the junction have a cross-section of 130 µm, while the outflow channel in the lower part of the flow cell (Figure 4A, light yellow) has a cross-section of 110 µm. However, the channels are originally designed (File S2, Supporting Information) to have a cross-section of 200 µm, which is larger than the 3D-printed channels.

To confirm the applicability of a multi-material microfluidic device with a hydrophobic outflow channel for W/O emulsion formation and to test whether the wettability switch between the 3D-printed parts is set correctly at the droplet-forming microchannel junction, Milli-Q-water is injected as the inner phase, and HFE 7500 mixed with 1.8% (w/w) ammonium salt of Krytox FSH as the surfactant is injected as the outer phase. The flow rates of the inner and outer emulsion phase are set to Q_d = 400 µL h^{-1} and Q_c = 2000 µL h^{-1}, respectively. At the microfluidic junction, droplets are formed in a uniform fashion with a size of d = 111 µm ± 2 µm and a frequency of 155 Hz ± 17 Hz (corresponding calculations can be found in the Supporting Information). However, at this point, we still see a need for improving the transparency of the microfluidic devices as it is challenging to follow droplet formation at the junction (compare respective video of droplet formation, Video S1, Supporting Information).

3.5. Oil-in-Water Emulsion Formation in 3D-Printed Flow Cells with Hydrophobic–Hydrophilic Pattern

Similar to 3D-printing multi-material flow cells with a hydrophilic-hydrophobic surface pattern, we also fabricate microfluidic devices with the inverted surface pattern for forming O/W emulsion droplets. Again, the change of 3D-printed materials is set to occur at the droplet-forming junction to ensure a hydrophilic surface following the outflow channel, thus avoiding microchannel wetting by the to-be-encapsulated oil phase. Since our results gathered by this point show that the wetting of uncured resin RF 2 is not complete on the surface of polymerized RF 3, therefore, preventing RF 2 to be coherently printed onto the surface of RF 3, the order of resins stays the same, but we change the orientation of the microchannels at the printing platform. The flow cell is rotated by 180° such that the outflow channel is printed first, then the second part containing the inflow ports is added by printing RF 3 to the RF 2-based part of

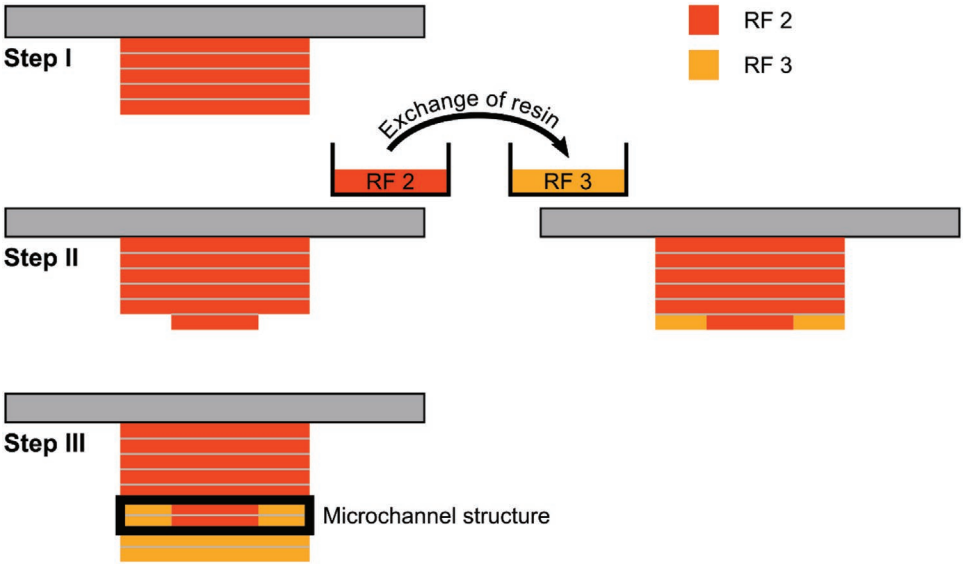

Figure 5. Scheme of the 3D printing process for combining two resins with opposite wettability. First, hydrophilic RF 2 is printed up to the region of interest (Step I). Here, in Step II, the object is printed layer- and voxelwise starting with RF 2. Then, the resin vat is exchanged for a vat containing RF 3 to complete the printing of the object layer. By repeating this process, a multimaterial object is obtained. Finally, the printing process is completed by addition of layers of RF 3 in Step III.

the flow cell (Figure 4B). The design is the same as in Section 3.4 (File S2, Supporting Information). Here, the dispersed channel has a cross-section of 185 µm and the outflow channel of 140 µm.

This way, the microchannels are hydrophilic at the droplet-forming nozzle, while the microchannels connecting the inflow ports and the nozzle are hydrophobic. For the formation of O/W emulsions, HFE 7500 is used as the inner phase and water with Triton X-100 ($c > 2.5 \times 10^{-4}$ M) as the surfactant is used as the outer phase. The flow rates are adjusted to $Q_d = 2000$ µL h^{-1} (inner phase) and $Q_c = 6000$ µL h^{-1} (outer phase) to yield droplets being 103 µm ± 6 µm in diameter at a frequency of 977 Hz ± 349 Hz. The droplet diameter is slightly smaller and reveals a higher standard deviation compared to the previously generated W/O emulsions with the same microchannel geometry (Section 3.4). We contribute this to the challenge of precisely adjusting the flow rates due to insufficient transparency and contrast of the 3D-printed materials. Thus, it is challenging to follow droplet formation inside the device as easily as in conventional PDMS-based microfluidics.

3.6. 3D-Printing of Microfluidic Devices with Spatially Controlled Wettability for Complex Emulsion Formation

As shown in Sections 3.4 and 3.5, we can process hydrophobic and hydrophilic resins into one material by 3D-printing RF 3 onto a surface made from RF 2. However, this method fails for more complex microchannel geometries and wettability patterns, respectively. For example, another hydrophilic part cannot be added to a pre-fabricated material with hydrophilic-hydrophobic pattern by changing the resin due to the insufficient wetting of RF 2 on the surface of RF 3. However, we require complex wettability patterns for several applications such as complex emulsion formation. In conventional microfluidics, several approaches have been proposed to obtain a tailored wettability pattern such as localized plasma treatment of the channel walls,[44] laminar flow patterning,[24] and layer-by-layer deposition of polyelectrolytes.[45] On this account, we develop a method to print a region of interest within a 3D object, and a microfluidic device in particular, in a layer-by-layer fashion based on the vat-switching technique by Choi et al.,[46] where surface properties can be addressed on a single-voxel basis (**Figure 5**).

We start with processing material RF 2 to form a stable basis at the printing platform for the region of interest (Step I). At this point, we continue to use RF 2 to print one more locally structured layer followed by an exchange of the resin vat to print RF 3 around the cured layer of RF 2 at the same Z-position and thus within the same layer (Step II light-yellow layer). By repeating Step II several times, an object is built with a hydrophilic section surrounded by two hydrophobic sections. Finally, the 3D-printed object is completed by finishing the object with several layers of RF 3 (Step III). To ensure that the resins do not mix when the bath is changed, the unpolymerized resin at the object is removed manually after each printing step by using a tissue to absorb the liquid resin via capillary forces. Further, Seiffert et al. showed that the penetration of oligomers into a polymerized network is poor and therefore, we expect only limited diffusion of uncured resin across the polymerized material.[47,48] Besides the fabrication of a microfluidic chip with spatially controlled wettability in the described fashion, it is also possible to print wettability patterns combining different materials as long as one material wets on the other. To prove this, we print a 3 × 3 chessboard-like pattern with a single-field length of 5 mm as shown in the Supporting Information (Video S2, Figure S4, Supporting Information). Despite the capability of 3D printing our resins with lower minimal feature size, we choose this length scale to easily handle the 3D-printed object.

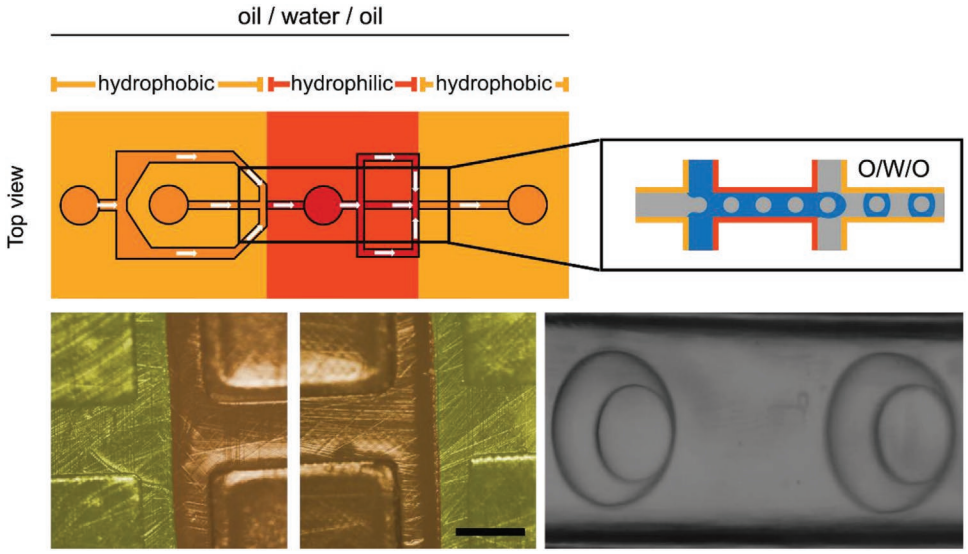

Figure 6. Schematic of a double emulsion device made via PμSL printing from two different materials with individual wettability. By manufacturing a surface pattern that is hydrophobic–hydrophilic–hydrophobic, O/W/O double emulsions can be formed inside the planar microchannels. In the lower row, a bright-field microscopy image of both junctions is shown. The hydrophobic material is colored in light-yellow and the hydrophilic material in reddish. The successful formation of double emulsions is followed inside the tubing of the outflow port (bottom right: Bright-field microscopy image of two double emulsion droplets). The scale bar denotes 300 μm.

To prove the locally controlled wetting, a droplet of water is placed on the surface of the chessboard-like pattern, and the water only spreads on the hydrophilic parts, while it dewets from the hydrophobic parts within seconds (Video S2, Supporting Information).

We apply our spatially controlled 3D printing approach to design a microfluidic device with a hydrophobic–hydrophilic–hydrophobic wettability pattern and utilize this flow cell for double emulsion formation (**Figure 6**). Compared to the single emulsion devices (Sections 3.4 and 3.5), we add a second microchannel junction and rotate the object by 90° to the building platform such that the channels are aligned in X, Y- instead of Z-direction and can thus be printed by the above-described method (Figure S5, Supporting Information). We also take advantage of the design freedom of PμSL printing and design the inflow microchannels of the outer phase to be on another level as the inner- and middle-phase inflow channels to compact the overall microchannel design. The hydrophilic part is located in the middle of the microfluidic device (scheme in Figure 6). The first part of the object is printed with RF 2 (exposure time t_{ex} = 1.5 s) up to two layers before the microchannel structure. At this point, only the hydrophilic part is printed with RF 2, and the resin is exchanged layer- and voxel-wise to print the remaining space within a layer with RF 3 at an exposure time of t_{ex} = 3 s. The microchannels are designed to be 400 μm in width and height. As the layer thickness is 50 μm, we print twelve layers using this method: two layers before the microchannels, eight layers containing the microchannels, and two more after the microchannel-carrying layers. The 3D-printing process is completed by manufacturing the remaining volume of the microfluidic device with RF 3. Pictures of both the 3D-printed device and bright-field microscopy images are shown in Figure S6, Supporting Information. It can be seen that the flow cell is not flat at the top. This is a result of insufficient support structures. Since the upper part of the flow cell has no further significance for the emulsion formation process, it is only a cosmetic defect and thus negligible. Measurements of the microchannel cross-sections show dimensions of 330 μm.

For forming O/W/O double emulsions, we inject HFE 7500 mixed with the ammonium salt of Krytox FSH (1.8% w/w) as the inner phase at a flow rate of Q_i = 4000 μL h^{-1}. Deionized water is mixed with Pluronic F-127 as the surfactant and serves as the middle phase with a flow rate of Q_m = 6000 μL h^{-1}. O/W single emulsions formed with this fluid pair are encapsulated by another outer phase, which is the same as for the most inner emulsion phase with a flow rate of Q_o = 8000 μL h^{-1}. A corresponding set of double emulsions passing through the outflow tubing is shown in Video S3, Supporting Information. By counting the number of different emulsion fractions, we calculate the respective percentage of the different droplet populations. We yield double emulsion droplets with a diameter of 282 ± 8 μm (deviation: 2.8%) with both one (51.9%) and two encapsulated oil cores (19.5%), and we also randomly observe single W/O emulsion droplets (28.6%), as shown in Figure S7, Supporting Information. In addition, mixing of the inner and outer oil phase can partially be observed resulting from insufficient stabilization of the double emulsion. While we are aware that the flow rates have to be tailored to ensure synchronized droplet formation at both junctions and thus quantitative double emulsion formation, again, the imperfect transparency of the 3D-printed flow cells hinders the view on the droplet formation process at each junction. By removing the dripping instability at the first microchannel junction and encapsulate both the inner and middle phase of the double emulsion only at the second junction,[49] we expect to improve

the yield of double emulsions, which is in the focus of ongoing work.

4. Conclusion

We have developed and investigated homemade acrylate-based photopolymer formulations yielding different surface properties in PμSL-based multi-material printing, exemplarily shown for microfluidic devices that exhibit spatially controlled wettability. By adding AA to a photopolymer formulation containing PEGDA (PEGDA-250), Sudan 1, and TPO, the contact angle against water can be tuned from 0° (superhydrophilic) up to ≈51° (hydrophilic). As a second resin, we introduce a photopolymer formulation based on fluorinated acrylates, namely PPFDA, and PFHDA mixed with Sudan 1 in acetone, and TPO. The contact angle against water can be increased up to ≈127° by adding 95% (w/w) of PPFDA. The solvent resistance of objects 3D-printed from both resins is tested showing resistance against common solvents used in microfluidics with exception of chloroform, acetone, and THF, in which they reveal moderate swelling of 7% to 9% compared to around 38% (in THF) and 39% (chloroform) for PDMS.[42] Furthermore, we have investigated the contact angle of the materials against each other concluding that both resins can be processed into a two-material polymer object with different spatial surface wettability.

From these resins, we have manufactured microfluidic flow cells for the formation of both W/O and O/W emulsions, each with tailored surface properties. The microchannels of these devices are as small as 130 μm in width and height, respectively. W/O emulsions generated in a microfluidic device with a hydrophilic-hydrophobic surface pattern are 113 μm ± 2 μm in diameter and formed at a frequency of 155 Hz ± 17 Hz. O/W emulsions produced in a flow cell with a hydrophobic–hydrophilic surface pattern are slightly smaller with a diameter of 103 μm ± 6 μm, formed at a frequency of 977 Hz ± 349 Hz.

Finally, we have developed a voxel- and layer-selective PμSL printing routine to combine the two strongly dissimilar materials, one being hydrophobic and the other being hydrophilic, to fabricate a microfluidic device for double emulsion formation. Here, the hydrophilic part is in the middle of the flow cell layout and surrounded by the hydrophobic material without any defects or unfilled space in between. Eventually, O/W/O double emulsions are fabricated in those devices that can serve as templates for microcapsule formation, drug delivery, and optical materials. To the best of our knowledge, it is the first time that resins with a contact angle down to ≈51° against water, and resin with a contact angle of ≈127° are reported for high-resolution PμSL. All microfluidic experiments were performed for at least 15 min, and no leakage was detected for any experiments in any flow cell, indicating sufficiently strong bonding between the different materials.

Supporting Information

Supporting Information is available from the Wiley Online Library or from the author.

Acknowledgements

This project received funding from the European Research Council (ERC) under the European Union's Horizon 2020 research and innovation program (Grant agreement No. 852065). This research was funded in part by the Federal Ministry of Education and Research (BMBF, Biotechnology2020+: Leibniz Research Cluster, 031A360C), the Volkswagen Foundation ("Experiment!"), and the German Research Foundation (DFG, Research Training Group 1865: Hydrogel-based Microsystems). J.T. acknowledges support from the Dresden Center for Intelligent Materials (DCIM) by the Free State of Saxony and TU Dresden. Additionally, the authors thank Martin Schumann (TU Dresden) for designing the table of contents graphic.

Open access funding enabled and organized by Projekt DEAL.

Conflict of Interest

The authors declare no conflict of interest.

Data Availability Statement

The data that supports the findings of this study are available in the supplementary material of this article.

Keywords

emulsion formation, hydrophilic-hydrophobic, microfluidics, microstereolithography, multi-material, wettability

Received: January 26, 2021
Revised: June 16, 2021
Published online: July 21, 2021

[1] J. C. McDonald, D. C. Duffy, J. R. Anderson, D. T. Chiu, H. Wu, O. J. A. Schueller, G. M. Whitesides, *Electrophoresis* **2000**, *21*, 27.
[2] G. M. Whitesides, E. Ostuni, S. Takayama, X. Jiang, D. E. Ingber, *Annu. Rev. Biomed. Eng.* **2001**, *3*, 335.
[3] Y. Xia, G. M. Whitesides, *Angew. Chem., Int. Ed.* **1998**, *37*, 550.
[4] S. K. Sia, G. M. Whitesides, *Electrophoresis* **2003**, *24*, 3563.
[5] A. K. Au, W. Lee, A. Folch, *Lab Chip* **2014**, *14*, 1294.
[6] H. Gong, A. T. Woolley, G. P. Nordin, *Lab Chip* **2016**, *16*, 2450.
[7] R. D. Sochol, E. Sweet, C. C. Glick, S.-Y. Wu, C. Yang, M. Restaino, L. Lin, *Microelectron. Eng.* **2018**, *189*, 52.
[8] L. Donvito, L. Galluccio, A. Lombardo, G. Morabito, A. Nicolosi, M. Reno, *J. Micromech. Microeng.* **2015**, *25*, 035013.
[9] M. J. Männel, L. Selzer, R. Bernhardt, J. Thiele, *Adv. Mater. Technol.* **2019**, *4*, 1800408.
[10] M. D. Nelson, N. Ramkumar, B. K. Gale, *J. Micromech. Microeng.* **2019**, *29*, 095010.
[11] W. Shen, M. Li, C. Ye, L. Jiang, Y. Song, *Lab Chip* **2012**, *12*, 3089.
[12] R. D. Sochol, E. Sweet, C. C. Glick, S. Venkatesh, A. Avetisyan, K. F. Ekman, A. Raulinaitis, A. Tsai, A. Wienkers, K. Korner, K. Hanson, A. Long, B. J. Hightower, G. Slatton, D. C. Burnett, T. L. Massey, K. Iwai, L. P. Lee, K. S. J. Pister, L. Lin, *Lab Chip* **2016**, *16*, 668.
[13] T. Femmer, A. Jans, R. Eswein, N. Anwar, M. Moeller, M. Wessling, A. J. C. Kuehne, *ACS Appl. Mater. Interfaces* **2015**, *7*, 12635.
[14] Y.-S. Lee, N. Bhattacharjee, A. Folch, *Lab Chip* **2018**, *18*, 1207.
[15] A. Urrios, C. Parra-Cabrera, N. Bhattacharjee, A. M. Gonzalez-Suarez, L. G. Rigat-Brugarolas, U. Nallapatti, J. Samitier, C. A. DeForest, F. Posas, J. L. Garcia-Cordero, A. Folch, *Lab Chip* **2016**, *16*, 2287.
[16] M. J. Männel, C. Fischer, J. Thiele, *Micromachines* **2020**, *11*, 246.

[17] G. M. Whitesides, *Nature* **2006**, *442*, 368.
[18] A. R. Abate, D. A. Weitz, *Small* **2009**, *5*, 2030.
[19] N. Hauck, N. Seixas, S. P. Centeno, R. Schlüßler, G. Cojoc, P. Müller, J. Guck, D. Wöll, L. A. Wessjohann, J. Thiele, *Polymers* **2018**, *10*, 1055.
[20] E. Brouzes, M. Medkova, N. Savenelli, D. Marran, M. Twardowski, J. B. Hutchison, J. M. Rothberg, D. R. Link, N. Perrimon, M. L. Samuels, *Proc. Natl. Acad. Sci. U. S. A.* **2009**, *106*, 14195.
[21] E. Szántai, A. Guttman, *Electrophoresis* **2006**, *27*, 4896.
[22] I. K. Dimov, L. Basabe-Desmonts, J. L. Garcia-Cordero, B. M. Ross, A. J. Ricco, L. P. Lee, *Lab Chip* **2011**, *11*, 845.
[23] T. Heida, T. Köhler, A. Kaufmann, M. J. Männel, J. Thiele, *ChemSystemsChem* **2020**, *2*, e1900058.
[24] A. R. Abate, J. Thiele, M. Weinhart, D. A. Weitz, *Lab Chip* **2010**, *10*, 1774.
[25] Y.-H. Hwang, T. Um, J. Hong, G.-N. Ahn, J. Qiao, I. S. Kang, L. Qi, H. Lee, D.-P. Kim, *Adv. Mater. Technol.* **2019**, *4*, 1900457.
[26] Q. Ji, J. M. Zhang, Y. Liu, X. Li, P. Lv, D. Jin, H. Duan, *Sci. Rep.* **2018**, *8*, 4791.
[27] J. M. Zhang, E. Q. Li, A. A. Aguirre-Pablo, S. T. Thoroddsen, *RSC Adv.* **2016**, *6*, 2793.
[28] M. Männel, N. Hauck, J. Thiele, *Solvent-Resistant Microfluidic Devices made from PFHDA Resins by Micro-Stereolithography*, Vol. *11235*, SPIE, Bellingham, USA **2020**.
[29] X. Zheng, J. Deotte, M. P. Alonso, G. R. Farquar, T. H. Weisgraber, S. Gemberling, H. Lee, N. Fang, C. M. Spadaccini, *Rev. Sci. Instrum.* **2012**, *83*, 125001.
[30] J. M. Zhang, Q. Ji, H. Duan, *Micromachines* **2019**, *10*, 754.
[31] D. K. Patel, A. H. Sakhaei, M. Layani, B. Zhang, Q. Ge, S. Magdassi, *Adv. Mater.* **2017**, *29*, 1606000.
[32] L. Brandhoff, S. van den Driesche, F. Lucklum, M. J. Vellekoop, *Creation of hydrophilic microfluidic devices for biomedical application through stereolithography*, Vol. *9518*, SPIE, Bellingham, USA **2015**.
[33] G. Gonzalez, A. Chiappone, K. Dietliker, C. F. Pirri, I. Roppolo, *Adv. Mater. Technol.* **2020**, *5*, 1.
[34] A. Chiado, G. Palmara, A. Chiappone, C. Tanzanu, C. F. Pirri, I. Roppolo, F. Frascella, *Lab Chip* **2020**, *20*, 665.
[35] C. I. Rogers, K. Qaderi, A. T. Woolley, G. P. Nordin, *Biomicrofluidics* **2015**, *9*, 016501.
[36] K. Kowsari, B. Zhang, S. Panjwani, Z. Chen, H. Hingorani, S. Akbari, N. X. Fang, Q. Ge, *Addit. Manuf.* **2018**, *24*, 627.
[37] C. Warr, J. C. Valdoz, B. P. Bickham, C. J. Knight, N. A. Franks, N. Chartrand, P. M. Van Ry, K. A. Christensen, G. P. Nordin, A. D. Cook, *ACS Appl. Bio Mater.* **2020**, *3*, 2239.
[38] H. Gong, M. Beauchamp, S. Perry, A. T. Woolley, G. P. Nordin, *RSC Adv.* **2015**, *5*, 106621.
[39] H. Gong, B. P. Bickham, A. T. Woolley, G. P. Nordin, *Lab Chip* **2017**, *17*, 2899.
[40] C. I. Rogers, J. B. Oxborrow, R. R. Anderson, L.-F. Tsai, G. P. Nordin, A. T. Woolley, *Sens. Actuators, B* **2014**, *191*, 438.
[41] Z. Chu, S. Seeger, *Chem. Soc. Rev.* **2014**, *43*, 2784.
[42] J. N. Lee, C. Park, G. M. Whitesides, *Anal. Chem.* **2003**, *75*, 6544.
[43] J. Tsibouklis, P. Graham, P. J. Eaton, J. R. Smith, T. G. Nevell, J. D. Smart, R. J. Ewen, *Macromolecules* **2000**, *33*, 8460.
[44] S. C. Kim, D. J. Sukovich, A. R. Abate, *Lab Chip* **2015**, *15*, 3163.
[45] W.-A. C. Bauer, M. Fischlechner, C. Abell, W. T. S. Huck, *Lab Chip* **2010**, *10*, 1814.
[46] J.-W. Choi, H.-C. Kim, R. Wicker, *J. Mater. Process. Technol.* **2011**, *211*, 318.
[47] S. Seiffert, J. Thiele, A. R. Abate, D. A. Weitz, *J. Am. Chem. Soc.* **2010**, *132*, 6606.
[48] S. Seiffert, W. Oppermann, *Polymer* **2008**, *49*, 4115.
[49] A. R. Abate, J. Thiele, D. A. Weitz, *Lab Chip* **2011**, *11*, 253.